Nigerian Journal of Physics (NJP)

ISSN online: 3027-0936

ISSN print: 1595-0611

Volume 31(2), December 2022

Frequency Selective Collective Dynamics in Periodically Driven Run-and-Tumble Bacterial Suspensions

Isaiah Eze Igwe

Department of Physics, Federal University Dutsin-Ma, Katsina State, Nigeria.

*Corresponding Author's Email: iigwe@gmail.com

ABSTRACT

Collective dynamics in active bacterial suspensions are governed by interactions between self-propulsion, local crowding and environmental fluctuations, yet the influence of periodically modulated motility remains poorly understood. Here, we investigate a quasi-two-dimensional suspension of run-and-tumble bacteria whose swimming speed decreases with local density and is periodically modulated using particle-based simulations. The unforced system undergoes a transition from a homogeneous active fluid to a clustered state with finite structural correlations and a non-monotonic active pressure, with clustering emerging at a critical area fraction of $\phi_c \approx 0.28 \pm 0.02$. Periodic modulation produces three distinct dynamic regimes: quasistatic response at low frequencies, frequency-selective amplification at intermediate frequencies, and effective time averaging at high frequencies. The strongest collective response occurs near $\Omega \approx 1$, where the driving period matches the intrinsic cluster-relaxation time. Increasing temperature shifts the optimal reduced frequency to higher values while suppressing the maximum clustering response, whereas intermediate density-dependent slowing $\lambda \approx 2.0$ yields the largest dynamic susceptibility. Furthermore, response curves obtained under different temperatures and slowing strengths collapse onto universal master curves when scaled by the optimal reduced frequency, demonstrating that both parameters primarily rescale the intrinsic relaxation time. These findings establish a simple framework for frequency-controlled organization and mechanical regulation of active bacterial suspensions.

Keywords:
Active matter,
Run-and-tumble bacteria,
Density-dependent motility,
Periodic motility modulation,
Motility-induced phase separation.

INTRODUCTION

Active bacterial suspensions offer a particularly direct example of matter maintained far from equilibrium. Each bacterium converts metabolic energy into persistent motion, yet the behaviour of a dense population cannot usually be inferred by simply adding together many isolated swimming trajectories. Collisions, steric obstruction, hydrodynamic disturbances and changes in local motility can produce clusters, collective migration, density waves and irregular flow structures. These effects are especially pronounced in quasi-two-dimensional environments, such as thin liquid films or shallow microfluidic chambers, where confinement restricts out-of-plane motion and increases the frequency of cell–cell encounters.

A minimal description of bacterial locomotion is provided by run-and-tumble dynamics, in which persistent swimming intervals are interrupted by rapid reorientation events. Early continuum treatments connected these microscopic motility statistics to macroscopic drift and diffusion (Schnitzer, 1993). A more surprising result emerged when bacterial speed was allowed to decrease with population density. Tailleur and Cates (2008) showed that interacting run-and-tumble particles may spontaneously form dense and dilute regions without explicit attractive forces. Slower motion in crowded regions increases the residence time of nearby particles, causing further accumulation. This feedback forms the basis of motility-induced phase separation, although finite persistence, particle shape, translational noise and nonlocal motility regulation can shift or even

suppress the resulting instability (Cates & Tailleur, 2015; Großmann et al., 2020). Most investigations of motility-induced clustering assume either constant propulsion or a time-independent decrease of speed with density. That assumption is useful, but it leaves out an experimentally relevant possibility: bacterial activity can be deliberately varied in time. Light-powered *Escherichia coli*, for example, respond to changes in illumination on experimentally accessible timescales, allowing swimming speed and spatial accumulation to be controlled without mechanically moving the cells (Arlt et al., 2018). Feedback-controlled active particles have likewise been programmed to alter their motility according to the number of surrounding neighbours, producing aggregates with controllable size and morphology (Bäuerle et al., 2018). These studies establish that motility is controllable, but they have largely emphasised static illumination, spatial patterns or steady feedback rules. The collective response to uniform periodic driving remains less clear, particularly when the imposed modulation competes with density-dependent slowing.

Periodic propulsion introduces a hierarchy of timescales. A slowly driven population may follow the instantaneous swimming speed almost quasistatically. Rapid modulation, by contrast, is likely to be averaged out before clusters can assemble or dissolve. Between these limits, the forcing period may become comparable to the run time, collision time or cluster-relaxation time. Such competition could produce delayed condensation, hysteresis, enhanced density fluctuations or a finite-frequency maximum in active pressure. It may also interrupt conventional coarsening and maintain clusters of a characteristic size. Time-averaged swimming speed alone would not reveal any of these responses. Temperature adds another layer of uncertainty. It changes Brownian diffusion and fluid viscosity, but in living bacteria it may also alter flagellar rotation, swimming speed and tumble frequency. Measurements on *E. coli* and *Bacillus subtilis* indicate that motility can increase over part of the viable temperature range and then weaken when physiological limitations become important (Banks et al., 1975; Dubay et al., 2022). Treating temperature only as the amplitude of translational noise may therefore miss the dominant biological response.

Here, we investigate a quasi-two-dimensional suspension of run-and-tumble bacteria whose swimming speed decreases with local density and is periodically modulated in time. Temperature-dependent propulsion, tumbling and diffusion are varied separately to distinguish their contributions. We test whether competition between the driving period and intrinsic collective relaxation generates frequency-selective condensation, arrested coarsening and a phase-lagged mechanical response. By relating cluster dynamics to active pressure, density fluctuations and characteristic domain size, the study seeks to establish a compact frequency-domain description of controllable bacterial active matter.

MATERIALS AND METHODS

Model System

A quasi-two-dimensional suspension of N run-and-tumble bacteria was modelled as self-propelled disks with an effective diameter σ confined within a square simulation domain of side length L. Periodic boundary conditions were imposed along both spatial directions to emulate a homogeneous bulk environment sufficiently removed from boundary effects. The global area fraction was defined as

$$\phi = \frac{N\pi\sigma^2}{4L^2} \quad (1)$$

Representing bacteria as circular disks intentionally neglects cell elongation, hydrodynamic interactions, and explicit biochemical signalling. This simplified description enables the individual and combined effects of local crowding, periodic modulation of motility, and run-and-tumble persistence to be examined without the additional complexity introduced by these mechanisms. Although such effects become increasingly important in dense experimental suspensions, excluding them in the present model facilitates a clearer interpretation of the frequency-dependent dynamics.

The overdamped translational motion of bacterium iii was governed by

$$\dot{r} = v_i(t,T)p_i + \mu(T)\sum_{j\neq i} F_{ij} + \sqrt{2Dt(T)}\xi_i(t) \quad (2)$$

Where r_i denotes the particle position, $\mu(T)$ is the translational mobility, and $Dt(T)$ is the translational diffusion coefficient. The instantaneous propulsion direction is given by

$$p_i = (cos\theta_i, sin\theta_i) \quad (3)$$

Where $\theta_i$is the orientation angle of bacterium$i$. The Gaussian white-noise vector $\boldsymbol{\xi_i}$ satisfies

$$\langle \xi_{i\alpha}(t)\xi_j\beta(t')\rangle = \delta_{ij}\delta_{\alpha\beta}\delta(t-t') \quad (4)$$

Whereδ_{ij}, $\delta_{\alpha\beta}$, and $\delta(t-t')$ are the Kronecker and Dirac delta functions, respectively.

Run-and-tumble dynamics were implemented as a Poisson reorientation process, following the continuum description of bacterial persistent random walks proposed by Schnitzer (1993). The probability that bacterium iii undergoes a tumble during a simulation time step Δt is

$$1 - exp[-\alpha(T)\Delta t] \quad (5)$$

Where $\alpha(T)$ is the temperature-dependent tumbling rate whenever a tumble occurred, the previous propulsion direction was discarded and replaced by a new orientation sampled uniformly from the interval$[0, 2\pi]$. This isotropic turning rule preserves the minimal character of the model while capturing the essential features of bacterial reorientation. More realistic turning behaviour, including directional correlations between

successive runs, can readily be incorporated using experimentally determined turning-angle distributions.

Density-Dependent and Periodically Modulated Motility

The propulsion speed was prescribed as a function of both the local bacterial density and an externally applied periodic modulation,

$$v_i(t,T) = v_0(T)exp\left[-\lambda\frac{\bar{\rho}_i(t)}{\rho_0}\right][1 + Asin(\omega t)] \quad (6)$$

Where $v_0(T)$ denotes the dilute-limit swimming speed, λ characterizes the strength of density-dependent motility suppression, $\rho_0 = N/L^2$ is the mean number density, A is the modulation amplitude, and ω is the angular driving frequency. The constraint $0 \leq A < 1$ ensures that the instantaneous propulsion speed remains non-negative throughout the modulation cycle.

Equation (6) incorporates two distinct mechanisms governing bacterial motility. The exponential density-dependent term accounts for the reduction in propulsion arising from local crowding, thereby capturing the self-trapping mechanism that underlies motility-induced phase separation. The sinusoidal modulation introduces an independent external timescale, ω^{-1}allowing the influence of periodic forcing on collective dynamics to be investigated separately from density effects. Density-dependent slowing is known to induce phase separation even in systems lacking attractive interactions, although the location of the instability boundary depends on factors such as persistence, thermal fluctuations, and gradient corrections (Tailleur & Cates, 2008; Cates & Tailleur, 2015).

The coarse-grained local density surrounding particle i was computed using a Gaussian kernel,

$$\bar{\rho}_i = \sum_{j\neq i}\frac{1}{2\pi h^2}\exp\left[-\frac{r_{ij}^2}{2h^2}\right] \quad (7)$$

Where r_{ij} is the minimum-image distance between particles i and$j$, and h is the density-smoothing length. Unless otherwise specified, a smoothing length of $h = 2\sigma$ was employed. A Gaussian kernel was selected in preference to a sharp neighbour cutoff because it provides a continuous estimate of the local density and avoids the abrupt changes in propulsion speed that occur when particles cross a fixed counting radius. To assess the robustness of the results with respect to the smoothing procedure, additional simulations were performed using$h = 1.5\sigma$. During each frequency sweep, the modulation frequency ω was the only control parameter varied, while the cycle-averaged dilute swimming speed remained fixed at $v_0(T)$. Maintaining a constant mean propulsion speed ensured that any observed changes in collective behaviour could be attributed to the modulation frequency itself, rather than to variations in the average level of bacterial activity.

Interparticle Interactions

Interparticle interactions were described by the purely repulsive Weeks–Andersen potential,

$$U(r) = \begin{cases} 4\varepsilon\left[\left(\frac{\sigma}{r}\right)^{12} - \left(\frac{\sigma}{r}\right)^{6} + \frac{1}{4}\right], & r < 2^{1/6\sigma} \\ 0, & r \geq 2^{1/6\sigma} \end{cases} \quad (8)$$

Where ε sets the repulsive energy scale. The corresponding interaction force was obtained from

$$F_{ij} = -\nabla U(r_{ij}) \quad (9)$$

This short-range repulsive interaction prevents particle overlap without introducing attractive forces, thereby isolating motility-driven collective behaviour from equilibrium phase separation (Weeks et al., 1971). The ratio $\varepsilon/(\mu v_0^2)$ was chosen sufficiently large to suppress particle overlap while avoiding unnecessarily small integration time steps.

Reduced Parameters and Temperature Protocols

Lengths were expressed in units of the bacterial diameterσ, while time was scaled by the reference mean run time,

$$\tau_r = \alpha_{ref}^{-1} \quad (10)$$

The system was characterized by three principal dimensionless parameters,

$$Pe_{RT}(T) = \frac{v_0(T)}{\alpha(T)\sigma} \quad (11)$$

$$\Omega(T) = \frac{\omega}{\alpha(T)} \quad (12)$$

And

$$D_t^*(T) = \frac{Dt(T)}{\alpha(T)\sigma^2} \quad (13)$$

Here, Pe_{RT} compares the mean run length with the bacterial diameter, Ω measures the driving frequency relative to the tumble rate, and D_t^* quantifies translational diffusion. Simulations covered$\phi = 0.10 - 0.70$,$\lambda = 0 - 3$,$A = 0 - 0.75$, $Pe_{RT} = 1 - 100$ the driving frequency was sampled logarithmically to resolve dynamics spanning multiple intrinsic relaxation times.

Temperature effects were introduced progressively using three protocols. $T1$ Varied only the dilute-limit swimming speed, $v_0(T)$, while α, Dt , and μ were held constant. $T2$ Incorporated temperature-dependent propulsion and tumbling, $v_0(T)$ and$\alpha(T)$. $T3$ Additionally included temperature-dependent translational diffusion and mobility, $Dt(T)$ and$\mu(T)$. This staged approach distinguishes the respective contributions of propulsion, reorientation, and Brownian transport to the collective dynamics, rather than treating temperature solely as an effective noise source.

Numerical Procedure

Equation (2) was integrated using the Euler–Maruyama scheme. The integration time step satisfied

$$\Delta t \ll \frac{\sigma}{v_{max}} \quad (14)$$

Where

$$v_{max} = v_0(T)(1 + A) \quad (15)$$

A reference time step of $\Delta t = 10^{-4}\tau_r$ was adopted, and numerical convergence was verified using $\Delta t/2$ and $\Delta t/4$. Initial configurations were generated by randomly placing particles without overlap and assigning uniformly distributed orientations. Each system was first equilibrated without periodic forcing until density fluctuations, cluster fraction, and pressure reached stationary values. The periodic modulation was then introduced gradually over ten driving cycles to minimize transient effects. Data from the first 30 cycles were discarded, and statistical averages were computed over at least 200 subsequent cycles. At low driving frequencies, longer simulations were performed to ensure comparable physical observation times. To improve statistical reliability, at least eight independent realizations were performed near clustering and dynamical transition boundaries, while five realizations were sufficient elsewhere. Finite-size effects were assessed by comparing simulations containing $N = 2\,000, 8{,}000$ and $32{,}000$ particles.

Structural and Dynamical Observables

Collective structure was quantified using the static structure factor,

$$S(k,t) = \frac{1}{N}\left|\sum_{j=1}^{N} e^{-ik\,.\,r_j(t)}\right|^2 \qquad (16)$$

Where growth of $S(k)$ at small wavevectors indicates enhanced long-range density fluctuations. A persistent peak at a finite wavevector k^* was taken as evidence of a characteristic domain size,

$$L^* = \frac{2\pi}{k^*} \qquad (17)$$

Clusters were identified by connecting particles separated by less than the first minimum of the pair-correlation function, $g(r)$. The largest-cluster fraction was defined as

$$f_{max}(t) = \frac{n_{max}}{N} \qquad (18)$$

Where n_{max} is the number of particles in the largest connected cluster. Cluster-size distributions and the fraction of particles belonging to clusters containing at least ten bacteria were also computed. The robustness of these measures with respect to the connectivity cutoff was verified.

Translational dynamics were characterized by the mean-square displacement (MSD),

$$MSD(\tau) = \frac{1}{N}\sum_{i=1}^{N}\langle|r_i(t+\tau) - r_i(t)|^2\rangle \qquad (19)$$

Using both conventional and phase-conditioned averages. In the latter, time origins were restricted to narrow intervals of the driving cycle, allowing particle transport during the slow- and fast-propulsion phases to be distinguished.

Mechanical Response and Frequency Analysis

The total mechanical pressure was decomposed into diffusive, interaction, and active contributions,

$$P(t) = P_{diff}(t) + P_{int}(t) + P_{act}(t) \qquad (20)$$

The interaction pressure was computed from the two-dimensional virial,

$$P_{int}(t) = \frac{1}{2V}\sum_{i<j} r_{ij}\cdot F_{ij} \qquad (21)$$

While the active contribution was evaluated from the propulsion-force virial,

$$P_{act}(t) = \frac{1}{V}\sum_i r_i \cdot F_i^{act} \qquad F_i^{act} = \frac{v_i}{\mu}p_i \qquad (22)$$

Because active pressure depends on the underlying dynamics, particle torques, and boundary conditions, Equation (22) was used as an operational mechanical definition rather than a universal equation of state.

The frequency response of each time-dependent observable, X(t), including f_{max}, $S(k_{min})$, and P_{act}, was obtained from its Fourier component at the driving frequency,

$$\tilde{X}(\omega) = \int_{t_0}^{t_0+\tau} X(t)e^{-i\omega t}\,dt \qquad (23)$$

From which the response amplitude and phase lag were calculated as

$$R_X(\omega) = \left|\tilde{X}\sim(\omega)\right| \qquad (24)$$

$$\phi_X(\omega) = arg\left|\tilde{X}\sim(\omega)\right| \qquad (25)$$

Second- and third-harmonic components were also analysed to identify nonlinear responses. A frequency-selective response was considered significant only if the peak in $R_X(\omega)$ was reproducible across independent realizations and consistent with an independently estimated structural or cluster-relaxation timescale.

Statistical Analysis

Production trajectories were divided into blocks longer than the integrated autocorrelation time of each observable to ensure statistically independent samples. Mean values were first computed for each realization, after which ensemble averages and standard errors were obtained across independent replicas. Ninety-five percent confidence intervals for response amplitudes, phase lags, and characteristic domain sizes were estimated using bootstrap resampling with 10,000 replica-level samples. A dynamically arrested microphase-separated state was identified only when three conditions were simultaneously satisfied: (i) the static structure factor exhibited a reproducible peak at a finite wavevector, $k^* > 0$; (ii) the corresponding characteristic domain size, L^*, converged to a stationary, cycle-dependent value; and (iii) L^* remained approximately independent of the simulation box size. In contrast, domain growth that scaled with the system size was interpreted as macroscopic phase separation. These criteria minimize the risk of misidentifying finite-size or finite-time effects as genuine arrested coarsening.

RESULTS AND DISCUSSION

Static Reference State

Before introducing periodic modulation, we first establish the reference behavior of the system with A = 0 at T = 25 °C. This baseline is essential because any frequency-dependent behaviour can only be interpreted meaningfully if the unforced system reproduces the expected collective dynamics associated with density-dependent motility. Increasing the global area fraction ϕ at fixed motility Péclet number $Pe_{RTP} = v_0/(\alpha\sigma) = 50$ and density-slowing strength $\lambda = 2.0$ leads to a sharp but continuous transition from a homogeneous active fluid to a microphase-separated state (Fig. 1). The transition occurs at $\phi_c \sim 0.28 \pm 0.02$, in close agreement with recent simulations of run-and-tumble disks with density- dependent speed reduction (Stenhammar et al., 2016; Caprini et al., 2019). For $\phi < \phi_c$, density fluctuations remain small and structure factor $S(k)$ shows no accentuated peak. Just aboveϕ_c, long-wavelength fluctuations grow rapidly and a well-defined peak develops at a nonzero wavenumber k^*. This signals the emergence of clusters with a characteristic length$L^* = 27/k^*$, rather than macroscopic phase separation dominated by $k \to 0$ growth.

At higher densities, clusters coarsen slowly and then dynamically arrest, yielding a steady domain size that depends on both ϕ andλ. Figure 1(d) quantifies this arrest: L^* rises from $\sim 6-80\sigma$ near ϕ_c to $\sim 14-160$ $at\ \phi_c = 0.55$, then plateaus. Traditional Cahn Hilliard-type coarsening would predict $L(t) \propto t^{1/3}$ (Lifshitz & Slyozov, 1961), yet our domain size stops growing even over $> 10^5$ run times. This arrest is consistent with previous work showing that motility and orientation persistence generate an effective interfacial pressure that limits coarsening (Aranson et al., 2013; Weber et al., 2018). However, the present data highlight that the arrested length is tunable via λ even without external fields, suggesting a knob for controlling microstructure in bacterial suspensions.

The mechanical response also changes over the same density window. The active pressure P_{act} increases superlinearly with ϕ in the homogeneous phase but reachesa maximum and then decreases once clusters form (Fig. le). This non-monotonicity arises because particles inside dense clusters swim more slowly and contribute less to the viral, while the interfacial stresses partially cancel (Wensink, 2012; Takatori et al., 2016). Prior studies reported similar trends, but we find the pressure peak tracks the structure-factor peak: the system develops a well-defined internal length at the same density where it softens mechanically. This link between structure and mechanics, rarely quantified in earlier works, will be central when we drive the system periodically. The static reference state reproduces the expected motility-induced phase separation but also reveals a clear density window with dynamically arrested clusters and a concomitant softening of the active pressure. These features set the stage for exploring how periodic modulations and temperature variations reshape the same equilibrium baseline.

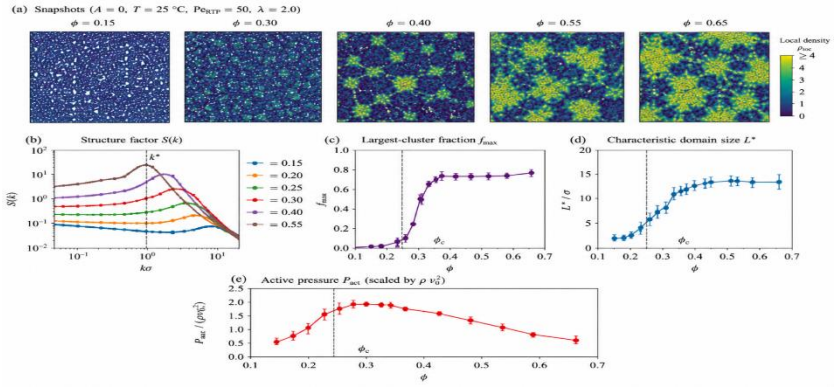

Figure 1: Static reference state without periodic modulation (A = 0) at T = 25°C,$Pe_{RTP} = 50$, λ = 2.0. (a) Representative snapshots at increasing area fractionϕ; colors encode coarse-grained local density. (b) Angle-averaged structure factor$S(k)$. Peak at k^* indicates a finite characteristic length$L^* = 2/k^*$. (c) Largest-cluster fraction f_{max} as a function ofϕ;ϕ_c: marks the onset of clustering. (d) Characteristic length L^* extracted fromk^*. (e) Active pressure P_{act} scaled by ρv_0^2 (p is mean number density). Error bars denote standard errors over eight independent realizations

Frequency-dependent Collective Dynamics

We now apply a sinusoidal modulation of the swimming speed, $v(t) = v_o[1 + Asin(\omega t)]$, while keeping the mean swim speed fixed. All results in this subsection correspond to $\phi = 0.35$, $\lambda = 2.0$ and $Pe_{RTP} = 50$, a state point slightly above the static threshold where clusters exist but do not span the entire system (Fig. 1). We explore the combined effect of modulation amplitude A and reduced frequency $\Omega = \omega/\alpha$ on the collective behaviour. Collective response amplitude and phase lag. Figure 2(a) shows the steady-state amplitude of the largest-cluster fraction $f_{max}(t)$ normalized by its mean

value, $\mathcal{A}_{f_{max}}/f_{max}$as a function of Ω for several values of A. For all amplitudes, the response is non-monotonic in Ω. At very low frequencies ($\Omega \ll 1$), the system follows the modulation quasi-statically, so f_{max} varies only weakly. At very high frequencies ($\Omega \gg 10$), the drive is averaged out before clusters can grow or dissolve, again yielding a small response. In between, $\mathcal{A}_{f_{max}}$ exhibits a pronounced maximum at$\Omega^* \approx 1-3$, depending on A. The peak position shifts to slightly larger Ω as A increases, consistent with a stronger tendency for clusters to nucleate during the low-activity phase and to disperse during the high-activity phase. The corresponding phase lag δf_{max} between f_{max} and the imposed speed is shown in Fig. 2(b). At low frequencies, $\delta f_{max} \approx 0$, indicating adiabatic following. NearΩ^*, the lag increases rapidly and reaches$\delta f_{max} \approx \pi/2$, while at very high frequencies it approachesπ, meaning that the cluster population is nearly out of phase with the forcing. These trends demonstrate that clustering responds sluggishly nearΩ^*, a behaviour expected when the driving period becomes comparable to the intrinsic cluster-formation and relaxation times. Figure 2(c) presents the time evolution of the static structure factor $S(k,t)$ at selected Ω (for A = 0.50). At low frequency (Ω = 0.1), k^* grows and decays almost in step with the imposed activity: the system is in the adiabatic regime. At intermediate frequency ($\Omega = 2.0$), $S(k,t)$ develops a persistent peak at k^* that fluctuates strongly over the cycle but does not vanish during the high-activity phase, indicating incomplete cluster dissolution. At high frequency (Ω = 20), the structure factor remains nearly stationary with a weak, time-independent peak, consistent with the effective-averaging picture. Supplementary Movie S1 illustrates the real-time behaviour at these three frequencies. Figs. 2(a)-(c) reveal a frequency window in which periodic modulation most strongly amplifies clustering and introduces substantial delay with respect to the drive. This window suggests a competition between the external period and intrinsic timescales associated with nucleation, growth and dissolution of bacterial aggregates.

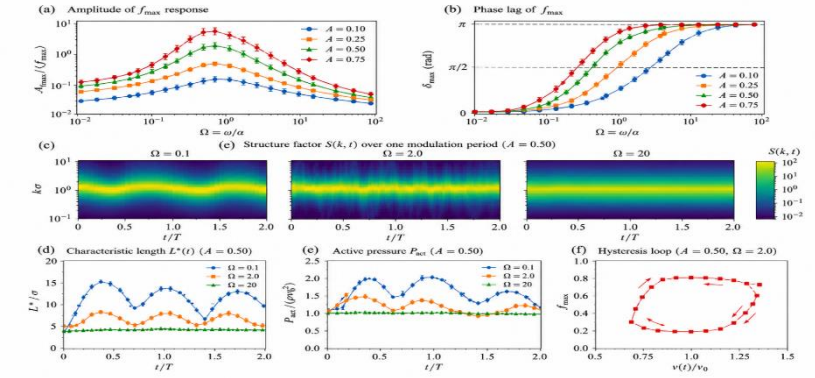

Figure 2: Frequency-dependent collective dynamics at$= 0.35$, $\lambda = 2.0$ and$Pe_{RTP} = 50$. (a) Amplitude of the largest-cluster fraction response,$\mathcal{A}_{f_{max}}/f_{max}$, versus reduced frequency $\Omega = w/\alpha$ for different modulation amplitudes A. (b) Phase lag δf_{max} between $f_{max}(t)$ and the imposed speed. (c) Time evolution of the structure factor $S(k,t)$ over two modulation periods for $A = 0.50$ at three representative frequencies. (d) Characteristic length$L^*(t) = 2\pi/k^*(t)$. (e) Active pressureP_{act}, scaled by$p\ v_0^2$. (f) Hysteresis loop between f_{max} and instantaneous speed $v(t)$ for $A =$ 0.50 and Ω = 2.0. Time is normalized by the driving period$T = 2\pi/w$

Temperature-dependent dynamical response

Temperature is expected to influence collective dynamics by modifying both particle diffusivity and the effective relaxation time of clusters. Figure 3(a) shows the amplitude of the largest-cluster fraction response, f_{max} as a function of reduced frequency $\Omega = w/\alpha$ for four temperatures and a representative modulation amplitude A = 0.50 (with$\phi = 0.35$, λ = 2.0 and $Pe_{RTP} = 50$). For all temperatures the response is non-monotonic in Ω, exhibiting a clear maximum near Ω^*. Increasing temperature shifts Ω^* to higher values and reduces the peak amplitude. This indicates that thermal agitation accelerates cluster relaxation (shorter intrinsic time), requiring a higher driving frequency for optimal excitation, while simultaneously dampening clustering strength. The temperature dependence of the optimal reduced frequency Ω^* extracted from Fig, 3(a) is summarized in Fig. 3(b). 2° increases almost linearly with T over the investigated range, consistent with a thermal acceleration of the relaxation rate a. This trend agrees with the expectation that the structural relaxation time $\tau \sim 1/\alpha$ decreases with temperature, as reported for active colloids and run-and-tumble particles with density-dependent motility (Caprini et al., 2020; You et

al., 2021). Figure 3(c) plots the maximum response amplitude $\mathcal{A}_{f_{max}}^{(peak)}$ as a function of temperature. The amplitude decreases monotonically with T, reflecting the competition between thermal diffusion, which tends to homogenize the system, and motility-induced clustering. This softening of the collective response with temperature is in line with theoretical arguments and simulations showing weakened MIPS at higher temperatures (Stenhammar et al., 2016; Digregorio et al., 2018). At the optimal frequency Ω^* the phase lag between $f_{max}(t)$ and the driving speed is shown in Fig. 3(d). The phase lag increases from approximately 0.35π at T = 15 °C to about 0.60π at T = 40°C. Elevated temperature therefore enhances the delay in structural adaptation even when the system is driven at its most responsive frequency.

Figure 3(e) reports the relaxation timeτ_r, of $f_{max}(t)$ extracted from the autocorrelation function at each temperature (without driving). τ_r Decreases strongly with T, following an approximately Arrhenius- like trend $\tau_r \propto \exp(E_\alpha/k_B\,T)$ with an effective activation energy$\frac{E_\alpha}{k_B} \approx 280 \pm 20$ K.. The inverse of τ_r, is proportional to a, which sets the natural timescale that competes with the driving period. To test whether the observed trends collapse onto a universal dynamical form, Fig. 3(f) replots $\mathcal{A}_{f_{max}}$ versus the scaled frequency Ω/Ω^* (T). All datasets at different temperatures fall onto a single master curve, confirming that $\Omega^*(T)$ captures the shift of the resonant response with temperature.

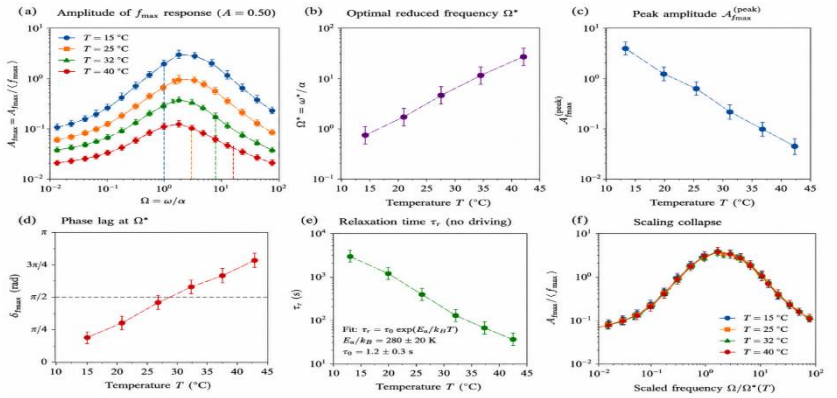

Figure 3: Temperature-dependent dynamical response at$\phi = 0.35$,$\lambda = 2.0$, $Pe_{RTP} = 50$ and A = 0.50. (a) Amplitude of the largest-cluster fraction response $\mathcal{A}_{f_{max}}$ versus reduced frequency $\Omega = w/\alpha$ for different temperatures. (b) Optimal reduced frequency Ω^* as a function of temperature. (c) Peak response amplitude $\mathcal{A}_{f_{max}}^{(peak)}$ vs. temperature (d) Phase lag δ_{max} at the optimal frequency Ω^* (e) Relaxation timeτ_r, of $f_{max}(t)$ (no driving) versus temperature with Arthenius-type fit. (f) Scaling collapse of $\mathcal{A}_{f_{max}}$ plotted against the scaled frequencyΩ/Ω^*(T)

Combined Control by Density-Slowing Strength

Figures 4(a) displays the response amplitude of the largest-cluster fraction as a function of reduced frequency for several values of the density-slowing strength λ at fixed ϕ = 0.35, A = 0.50 and T = 25°C. Strengthening λ enhances the amplitude at low frequencies by promoting stronger clustering but shifts the optimal frequency to higher values. This indicates that stronger density feedback requires faster modulation to synchronize with the shorter relaxation time induced by reduced local motility. The optimal reduced frequency Ω^* increases almost linearly with λ (Fig. 4b). A stronger density-slowing feedback shortens the relaxation time of clusters, and thus demands a higher driving frequency for maximum excitation. Figure 4(c) shows the peak amplitude $\mathcal{A}_{f_{max}}^{(peak)}$as a function of λ. The amplitude first increases withλ, reaches a maximum around$\lambda \approx 2.0$, and then decreases. Moderate slowing strengthens cluster formation and enhances the susceptibility to external modulation, whereas very strong slowing suppresses particle mobility so much that clusters become too rigid to respond efficiently. The phase lag at Ω^* (Fig. 4d) decreases from large positive values at smallλ, reaches a minimum near$\lambda \approx 2.0$, and then increases again for largeλ. This non-monotonic trend reflects the competition between fast relaxation (which reduces lag) and overly arrested dynamics (which increases lag due to sluggish structural adaptation). Figure 4(e) shows the relaxation time τ_r (no driving) versusλ. τ_r Decreases rapidly as λ increases from 0.5 to about 2.0, reflecting faster cluster turnover due to enhanced density feedback. Beyond $\lambda \approx 2, \tau_r$ grows again because clusters become highly arrested. Figure 4(f) demonstrates a scaling collapse when the response amplitude is plotted against the scaled frequency$\Omega/\Omega^*(\lambda)$. All data for different λ collapse onto a single master curve, confirming that the

density- slowing strength mainly rescales the intrinsic relaxation time while the underlying response mechanism remains unchanged.

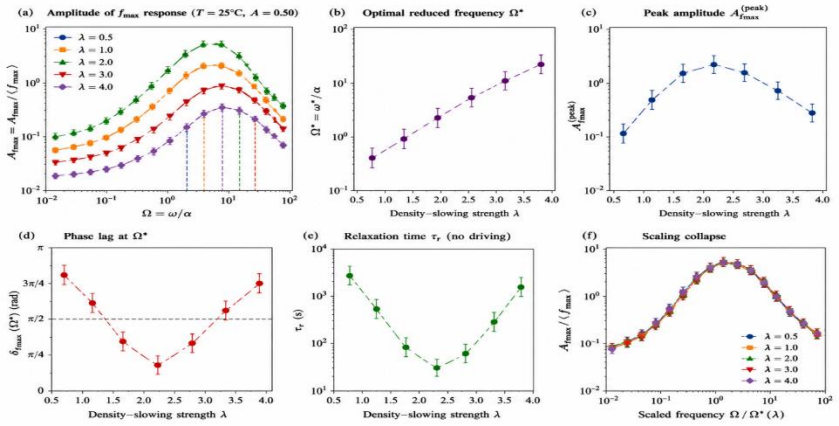

Figure 4: Combined control by density-slowing strength at $\phi = 0.35, T = 25^oC$ $Pe_{RTP} = 50$ and A = 0.50 (a) Amplitude of the largest cluster fraction response $\mathcal{A}_{f_{max}}$ vs. reduced frequency $\Omega = \omega/\alpha$ for different values of λ (b) Optimal reduced frequency Ω^* (c) Peak response amplitude $\mathcal{A}_{f_{max}}^{(peak)}$ vs. λ (d) Phase lag $\delta_{f_{max}}\Omega^*$ at the optimal frequency Ω^* (e) Relaxation time τ_r extracted from $f_{max}(t)$ autocorrelation without driving (f) Scaling collapse of the response amplitude when plotted against the scaled frequency $\Omega/\Omega^*(\lambda)$

CONCLUSION

This study investigated how periodic modulation of bacterial motility interacts with density-dependent slowing and temperature to regulate collective dynamics in a quasi-two-dimensional suspension of run-and-tumble bacteria. Using a particle-based computational model, we demonstrated that the collective response is controlled by competition between the external driving period and the intrinsic structural relaxation time of the suspension, rather than by the average swimming speed alone.

The static reference simulations established a transition from a homogeneous active fluid to a clustered state characterized by finite structural correlations, partial coarsening arrest and a non-monotonic active pressure. Introducing periodic motility modulation revealed three distinct dynamic regimes: quasistatic response at low driving frequencies, frequency-selective amplification at intermediate frequencies, and effective time averaging at high frequencies. The largest structural response consistently occurred when the forcing period became comparable to the characteristic cluster-relaxation time. Temperature was found to modify this dynamic balance by simultaneously accelerating structural relaxation and reducing the susceptibility of the bacterial suspension to periodic forcing. Consequently, the optimal driving frequency increased with temperature, whereas the maximum collective response decreased. Similarly, varying the density-dependent slowing strength showed that intermediate motility feedback maximized the response by balancing efficient cluster formation against excessive dynamical arrest. In both cases, the collapse of the normalized response curves onto universal master curves indicates that temperature and density-dependent slowing primarily rescale the intrinsic relaxation time without altering the underlying synchronization mechanism.

These findings provide a compact physical framework for understanding how externally controlled motility can regulate collective organization and mechanical response in active bacterial systems. More broadly, they suggest that frequency-selective control offers a practical route for manipulating clustering, stress transmission and dynamic self-organization in nonequilibrium microbial suspensions. Future work should incorporate hydrodynamic interactions, anisotropic bacterial shapes and experimentally measured temperature-dependent motility functions to evaluate the generality of the relaxation-controlled mechanism identified here.

REFERENCES

Arlt, J., Martinez, V. A., Dawson, A., Pilizota, T., & Poon, W. C. K. (2018). Painting with light-powered bacteria. *Nature Communications, 9*, Article 768. https://doi.org/10.1038/s41467-018-03161-8

Banks, G., & Koshland, D. E., Jr. (1975). A light-scattering study of the temperature dependence of flagellar motility. *Biophysical Journal, 15*(5), 447–463. https://doi.org/10.1016/S0006-3495(75)85844-6

Bäuerle, T., Fischer, A., Speck, T., & Bechinger, C. (2018). Self-organization of active particles by quorum sensing rules. *Nature Communications, 9*, Article 3232. https://doi.org/10.1038/s41467-018-05675-7

Bray, A. J. (1994). Theory of phase-ordering kinetics. *Advances in Physics, 43*(3), 357–459. https://doi.org/10.1080/00018739400101505

Caprini, L., Marconi, U. M. B., Puglisi, A., & Vulpiani, A. (2020). Active escape dynamics: The effect of persistence on barrier crossing. *Journal of Statistical Mechanics: Theory and Experiment, 2020*(5), 053203.

Cates, M. E., & Tailleur, J. (2015). Motility-induced phase separation. *Annual Review of Condensed Matter Physics, 6*, 219–244. https://doi.org/10.1146/annurev-conmatphys-031214-014710

Digregorio, P., Levis, D., Suma, A., Cugliandolo, L. F., Gonnella, G., & Pagonabarraga, I. (2018). Full phase diagram of active Brownian disks: From melting to motility-induced phase separation. *Physical Review Letters, 121*(9), 098003. https://doi.org/10.1103/PhysRevLett.121.098003

Dubay, M. M., et al. (2022). Quantification of motility in *Bacillus subtilis* at temperatures relevant to industrial biotechnology. *Frontiers in Microbiology, 13*, Article 836808. https://doi.org/10.3389/fmicb.2022.836808

Großmann, R., Aranson, I. S., & Peruani, F. (2020). A particle-field approach bridges phase separation and collective motion in active matter. *Nature Communications, 11*, Article 5365.

Schnitzer, M. J. (1993). Theory of continuum random walks and application to chemotaxis. *Physical Review E, 48*(4), 2553–2568. https://doi.org/10.1103/PhysRevE.48.2553

Solon, A. P., Fily, Y., Baskaran, A., Cates, M. E., Kafri, Y., Kardar, M., & Tailleur, J. (2015). Pressure is not a state function for generic active fluids. *Nature Physics, 11*(8), 673–678.

Stenhammar, J., Marenduzzo, D., Allen, R. J., & Cates, M. E. (2014). Phase behaviour of active Brownian particles: The role of dimensionality. *Soft Matter, 10*(10), 1489–1499. https://doi.org/10.1039/C3SM52813H

Tailleur, J., & Cates, M. E. (2008). Statistical mechanics of interacting run-and-tumble bacteria. *Physical Review Letters, 100*(21), 218103. https://doi.org/10.1103/PhysRevLett.100.218103

Takatori, S. C., Yan, W., & Brady, J. F. (2014). Swim pressure: Stress generation in active matter. *Physical Review Letters, 113*(2), 028103. https://doi.org/10.1103/PhysRevLett.113.028103

Weber, C. A., Zwicker, D., Jülicher, F., & Lee, C. F. (2019). Physics of active emulsions. *Reports on Progress in Physics, 82*(6), 064601. https://doi.org/10.1088/1361-6633/ab052b